Available online at www.sciencedirect.com
SCIENCE DIRECT®
International Journal of Thermal Sciences 43 (2004) 499–507
International Journal of Thermal Sciences
www.elsevier.com/locate/ijts

Investigation of a wire plate micro heat pipe array

Stéphane Launay [a], Valérie Sartre [a], Marcia B.H. Mantelli [b], Kleber Vieira de Paiva [b], Monique Lallemand [a,*]

[a] *CETHIL, UMR CNRS 5008, INSA, 20, av. A. Einstein, 69621 Villeurbanne Cedex, France*
[b] *Mechanical Engineering Department, Federal University of Santa Catarina UFSC, P.O. Box 476, Florianopolis, 88040-900, SC, Brazil*

Received 9 June 2003; accepted 14 October 2003

Abstract

In the present work, experimental and theoretical investigations have been conducted on a copper/water wire plate micro heat pipe (MHP). The experimental results show that its effective thermal conductivity is improved by a factor 1.3 as compared to the empty MHP array. A numerical model is used to predict the fluid distribution along the MHP axis, the temperature field and the maximum heat flux corresponding to the MHP capillary limit. The 1D, steady-state hydrodynamic model is based on the conservation equations for the liquid and vapour phases. The wall temperatures are calculated from the thermal resistance network of the wall and the liquid film. A good agreement between the theoretical and experimental data is achieved. The effect of various parameters—contact angle, fluid type, corner angle, fill charge—is theoretically investigated.

Keywords: Micro heat pipe array; Effective thermal conductivity; Capillary limit; Experimental study; Theoretical model

1. Introduction

Micro heat pipes (MHPs) are efficient cooling systems, which allow to transfer high heat fluxes and to reduce the temperature gradients. They are one of the most promising technologies in the field of thermal management of electronic components [1]. The MHP is a heat pipe in which the interfacial radius of curvature has the same order of magnitude than the tube hydraulic radius. The tube, of non-circular cross-section, has a transversal dimension of about 10 μm to 1 mm and a length of a few centimeters. The heat flux applied to the evaporator region vaporises the working fluid and the resulting vapour flows to the condenser through the adiabatic region of the heat pipe. The vapour then condenses, releasing the latent heat of condensation. In a transversal cross-section, the interfacial forces pull the liquid in the sharp angle corners, forming menisci. Due to the evaporation and condensation processes, the liquid–vapour interface curvature varies continuously from the condenser to the evaporator. This results in a pressure difference between both regions that involves the fluid flow from the condenser back to the evaporator.

Due to their small size, special techniques should be used to manufacture MHPs. Microgrooves have been machined in metallic foils [2] or metallic plates [3] with a diamond saw. Another technique consists of bonding an array of parallel metal wires sandwiched between two thin metal sheets [4]. These MHPs may have enhanced thermal performance or not; it all depends on the brazing material in the grooves formed between the wires and the plates [5]. For lower sizes, the MHP arrays are usually etched into silicon wafers. Parallel grooves [6–8] or radial grooves [9] of triangular or trapezoidal cross-sectional shapes are obtained by anisotropic etching in a KOH aqueous solution, and 3D rectangular grooves by deep plasma etching. The channels are closed by molecular or eutectic bonding of a silicon wafer.

In the present work, a wire plate MHP was developed using the diffusion welding fabrication process. The MHP has been experimentally tested at the Federal University of Santa Catarina (Brazil). A numerical model of this wire plate MHP array has been developed at the Centre of Thermal Sciences of Lyon (France). One objective of this study is to validate the numerical model with the experimental data. This model is used to analyse the hydrodynamic and thermal behaviour of this type of MHP array.

* Corresponding author.
E-mail addresses: launay@cethil.insa-lyon.fr (S. Launay), sartre@cethil.insa-lyon.fr (V. Sartre), marcia@emc.ufcs.br (M.B.H. Mantelli), m.lal@cethil.insa-lyon.fr (M. Lallemand).

1290-0729/$ – see front matter
doi:10.1016/j.ijthermalsci.2003.10.006

Nomenclature

A	section area	m^2	
g	gravitational constant	$m{\cdot}s^{-2}$	
h_{lv}	latent heat of vaporisation	$J{\cdot}kg^{-1}$	
l	minimum spacing between two wires	m	
L	length	m	
Ma	Mach number		
P	pressure	Pa	
Q	heat transfer rate	W	
q	lineic heat flux	$W{\cdot}m^{-1}$	
R	meniscus curvature radius	m	
R_{th}	thermal resistance	$K{\cdot}W^{-1}$	
r	copper wire radius	m	
T	temperature	K	
u	velocity	$m{\cdot}s^{-1}$	
x	abscissa	m	

Greek symbols

α	contact angle	degree
θ	inclination angle	degree
ρ	density	$kg{\cdot}m^{-3}$
σ	surface tension	$N{\cdot}m^{-1}$
τ	shear stress	Pa
φ	angle defined in Fig. 3	degree
φ_C	half angle of the corner defined in Fig. 3	degree

Subscripts

a	adiabatic section
c	cooled zone
C	corner
d	dry-out
f	flooding
h	heated zone
i	interface
l	liquid
m	melting
max	maximum
min	minimum
sat	saturation
v	vapour
t	total
w	wall

2. Fabrication process

If the very sharp angle between a plate and a cylinder can be welded without blocking the groove, the angle can work as an efficient porous medium for heat pipe applications. This can be done by diffusion welding.

The solid state diffusion is a welding process in which atomic diffusion, activated by high temperature levels and controlled by the pressure applied between the surfaces, induces a very strong junction. The main disadvantage of the diffusion welding, when compared to the traditional welding processes, is that the thermal cycle necessary for a proper welding can be too long. That is why the production is limited and its costs is high. Another limitation concerns the geometry of the surfaces to be welded [10,11].

Typically, the diffusion is realised between $0.5–0.8T_m$, where T_m is the melting temperature of the basis material. For copper, the process shows optimum results for temperatures ranging between 450 °C and 820 °C, depending on the geometry of the samples, the applied specific pressure and the welding time [12]. The atmosphere is also an important parameter. Usually, copper plates are welded in high-vacuum environment, but an inert or reduced atmosphere can also be used.

For the MHPs investigated, the selected temperature for diffusion welding is equal to 850 °C [5]. The vacuum level is about 10^{-4} mbar. The pressure to be applied depends on the geometry of the MHP and a special device was designed and constructed for the MHP welding. This device takes the advantage of the difference between the thermal expansion properties of the copper and of the stainless steel so that, as the temperature increases, the applied pressure also increases.

To guarantee a good welding, the wires and the flat plate must be cleaned with a 10% sulphuric acid solution to remove any oxidation that could block the copper diffusion, before the thermal cycle. Flowing water is used to rinse the wires and the plate, for about 10 min.

After the welding, acetone is introduced in the MHP to wash the grooves. The MHP is then vacuum tested using a leak detector, charged with the selected working fluid and sealed. After the charging, the MHP is ready for experimental study.

3. Experimental study

3.1. MHP array geometry

The investigated MHP array, consisting in three individual MHPs, is 78 mm long, 10 mm wide and 2.05 mm thick. The wire diameter is 1.45 mm and the plate thickness is 0.3 mm. Due to the welding, a 17°-value is estimated for the corner angles. The MHP is filled with 143 mm^3-distilled water, a volume equivalent to 23% of the MHP internal volume (at 20 °C). A cross-sectional view of the MHP array is shown in Fig. 1.

With a hydraulic diameter greater than 1 mm, this heat pipe can be considered as a mini heat pipe [13]. Nevertheless, this system operates like a micro heat pipe, using the sharp corners formed between the wires and plates as capillary structure. The MHP is tested in a horizontal

position where the effect of the gravity forces can be neglected. The heated section has a length of 25 mm. The heat input is delivered by means of an electrical resistance, wound around the evaporator. The heat flux is uniformly imposed along the axial heating length. The adiabatic section, 20 mm long, is thermally insulated with glass fiber and the cooled section length is 33 mm. For the condenser, the inlet cooling water temperature, controlled by a thermal bath, is kept constant and equal to 300 ± 0.01 K.

The wall temperature along the tube is measured by means of six T-Type thermocouples (Fig. 1), which are set on kapton tapes. The uncertainty of the temperature measure is ± 1 K.

3.2. Experimental results

The experimental temperature distributions of a charged MHP array and an empty one with no working fluid are shown in Fig. 2 at steady state. The experimental conditions are the same in both tests. The performance of a MHP array is characterised by its capacity to transfer heat from the heated zone to the cooled one, with a low temperature gradient. The better is its performance, the higher is its thermal conductivity. Comparing the temperature gradients of the empty and the charged MHP (Fig. 2), the overall thermal conductivity of the charged MHP array is shown to be 1.3 times greater than the empty array one.

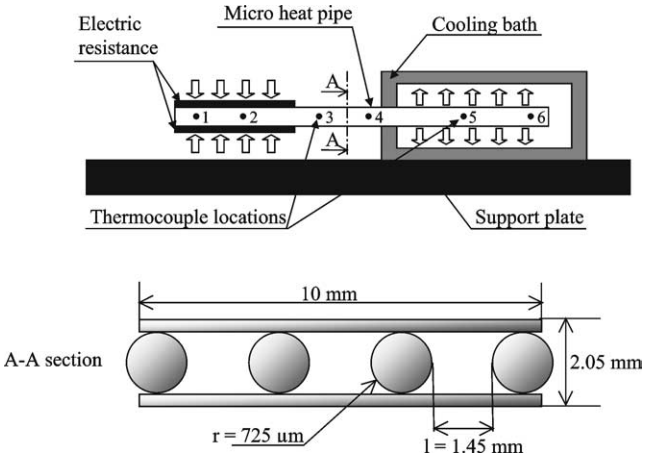

Fig. 1. Schematic view of the wire plate MHP array and thermocouple locations.

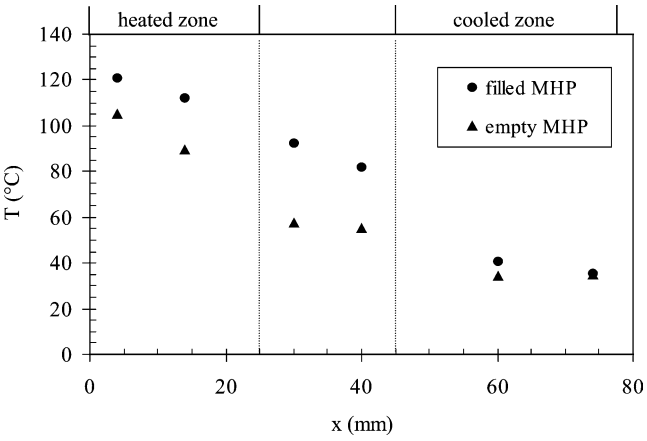

Fig. 2. Comparison of the axial temperature distributions for the charged and empty MHPs.

4. Numerical model

Many models have been developed in the literature to predict the capillary limit and the optimum fill charge of MHP arrays. Isothermal hydrodynamic models are based on the conservation equations of each phase. Among the various cross-sectional geometries of the MHP investigated, the most usual one is the triangular shape [14–17], but also square [18] and trapezoidal cross-sections [19] have been studied. Recently, Wang and Peterson [4] developed a steady-state, one-dimensional liquid–vapour flow model to predict the capillary limit of a wire-bonded aluminium/acetone MHP array, similar to the MHP investigated in this study.

In the present numerical model, both the hydrodynamic model of Wang and Peterson [4] and a heat transfer model in the MHP wall, have been developed for a wire plate copper/water MHP array. This model is used to predict the capillary limit and the temperature profile along the MHP as a function of the boundary conditions (imposed heat flux in the heated zone, third kind boundary condition in the cooled zone) and of the fill charge.

4.1. Hydrodynamic model

In the present hydrodynamic model, the conservation equations account for the axial variation of the liquid and vapour cross-sectional area and of the meniscus curvature radius. The MHP is divided into small control volumes of length dx for which the conservation laws are applied. The modelled geometry shown in Fig. 3 takes into account the

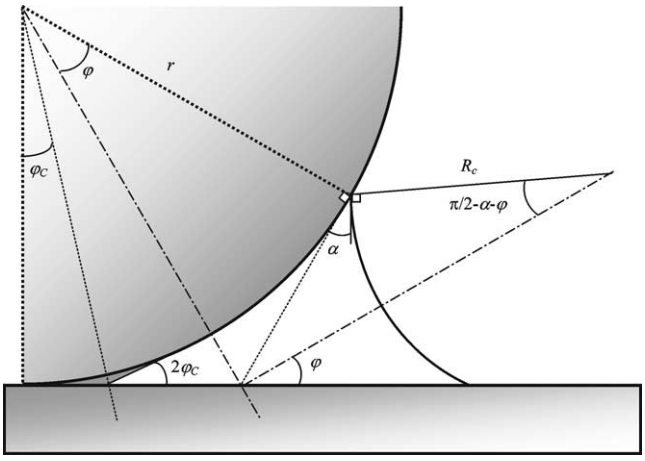

Fig. 3. Cross-sectional view of the liquid meniscus.

MHP symmetries. The hypotheses of the present model are those of Longtin et al. [16]:

- the liquid–vapour flow is incompressible ($Ma \ll 1$),
- the vapour and wall temperatures only vary along the axial direction (x-axis),
- the heat flux is uniformly distributed along the heated zone.

4.1.1. Geometrical parameters

In the conservation equations, geometrical parameters are needed, like the liquid and vapour cross-sectional area, A_l and A_v, respectively, the liquid–vapour interfacial area A_i and the wall surface area in contact with the liquid and the vapour, A_lw and A_vw, respectively. These parameters depend on the contact angle and the corner angle. The cross-sectional area of the liquid is:

- if $\varphi > \varphi_\mathrm{C}$

$$A_\mathrm{l} = 4\left\{r^2[\tan\varphi - \tan\varphi_\mathrm{C} - \varphi + \varphi_\mathrm{C}] + R^2\left[\frac{\cos^2\Psi}{\tan\varphi} - \frac{\pi}{2} + \Psi + \frac{\sin 2\Psi}{2}\right]\right\} \quad (1)$$

$$\Psi = \varphi + \alpha$$

- if $\varphi < \varphi_\mathrm{C}$

$$A_\mathrm{l} = 4\left\{R^2\left[\frac{\cos^2(\varphi_\mathrm{C}+\alpha)}{\tan\varphi_\mathrm{C}} - \left(\frac{\pi}{2} - \varphi_\mathrm{C} - \alpha - \frac{\sin 2(\varphi_\mathrm{C}+\alpha)}{2}\right)\right]\right\} \quad (2)$$

with r the copper wire radius, R the meniscus curvature radius, α the contact angle, φ_C the half-angle of the corner formed between a plate and a wire and φ the angle defined in Fig. 3. φ can be expressed as a function of r and R as:

$$\varphi = \arctan\left(-\frac{1}{2}\frac{R}{r}\sin\alpha + \sqrt{\left(\frac{1}{2}\frac{R}{r}\sin\alpha\right)^2 + \frac{R}{r}\cos\alpha}\right) \quad (3)$$

The cross-sectional area of the vapour is:

$$\begin{aligned} A_\mathrm{v} &= A_\mathrm{t} - A_\mathrm{l} \\ A_\mathrm{v} &= r^2\big[4 - \pi - 4(\tan\varphi_\mathrm{C} - \varphi_\mathrm{C})\big] + 2rl - A_\mathrm{l} \end{aligned} \quad (4)$$

where A_t is the MHP total cross-section ($A_\mathrm{l} + A_\mathrm{v}$) and l the minimum spacing between two copper wires.

The liquid–wall, vapour–wall contacting surface areas and the interfacial area, $\mathrm{d}A_\mathrm{lw}$, $\mathrm{d}A_\mathrm{vw}$ and $\mathrm{d}A_\mathrm{i}$, respectively, are expressed for a control volume of length $\mathrm{d}x$:

$$\mathrm{d}A_\mathrm{lw} = 4\big[2r(\tan\varphi + \varphi - \varphi_\mathrm{C})\,\mathrm{d}x\big] \quad (5)$$

$$\mathrm{d}A_\mathrm{vw} = 4\big[2\pi r + 2(l+2r)\big]\mathrm{d}x - \mathrm{d}A_\mathrm{lw} \quad (6)$$

$$\mathrm{d}A_\mathrm{i} = 4\big[\pi - 2(\varphi - \alpha)\big]R\,\mathrm{d}x = \beta_i R\,\mathrm{d}x \quad (7)$$

4.1.2. Mass balance

For the liquid flow, the mass balance is expressed by:

$$A_\mathrm{l}\frac{\mathrm{d}u_\mathrm{l}}{\mathrm{d}x} + \beta u_\mathrm{l}\frac{\mathrm{d}R}{\mathrm{d}x} = -\frac{q}{\rho_\mathrm{l} h_\mathrm{lv}} \quad (8)$$

where $\beta = \frac{\mathrm{d}A_\mathrm{l}}{\mathrm{d}x}\left(\frac{\mathrm{d}R}{\mathrm{d}x}\right)^{-1} \cdot q$ is the heat flux, equal to Q/L_h in the heated section, 0 in the adiabatic section and Q/L_c in the cooled section.

For the vapour flow, the mass balance is expressed by:

$$A_\mathrm{v}\frac{\mathrm{d}u_\mathrm{v}}{\mathrm{d}x} - \beta u_\mathrm{v}\frac{\mathrm{d}R}{\mathrm{d}x} = \frac{q}{\rho_\mathrm{v} h_\mathrm{lv}} \quad (9)$$

4.1.3. Momentum balance

For the liquid phase, the momentum balance can be written:

$$2\rho_\mathrm{l} u_\mathrm{l} A_\mathrm{l}\frac{\mathrm{d}u_\mathrm{l}}{\mathrm{d}x} + \beta\rho_\mathrm{l} u_\mathrm{l}^2\frac{\mathrm{d}R}{\mathrm{d}x} + A_\mathrm{l}\frac{\mathrm{d}P_\mathrm{l}}{\mathrm{d}x} = \beta_\mathrm{i} R|\tau_\mathrm{i}| + \frac{\mathrm{d}A_\mathrm{lw}}{\mathrm{d}x}|\tau_\mathrm{lw}| - \rho_\mathrm{l} g A_\mathrm{l}\sin\theta \quad (10)$$

where β_i is defined in Eq. (7) and for the vapour phase:

$$2\rho_\mathrm{v} u_\mathrm{v} A_\mathrm{v}\frac{\mathrm{d}u_\mathrm{v}}{\mathrm{d}x} - \beta\rho_\mathrm{v} u_\mathrm{v}^2\frac{\mathrm{d}R}{\mathrm{d}x} + A_\mathrm{v}\frac{\mathrm{d}P_\mathrm{v}}{\mathrm{d}x} = -\beta_\mathrm{i} R|\tau_\mathrm{i}| - \frac{\mathrm{d}A_\mathrm{vw}}{\mathrm{d}x}|\tau_\mathrm{vw}| - \rho_\mathrm{v} g A_\mathrm{v}\sin\theta \quad (11)$$

4.1.4. Laplace–Young equation

The first curvature radius of the meniscus is given by the Laplace–Young equation:

$$\frac{\mathrm{d}P_\mathrm{l}}{\mathrm{d}x} = \frac{\mathrm{d}P_\mathrm{v}}{\mathrm{d}x} - \frac{\mathrm{d}}{\mathrm{d}x}\left(\frac{\sigma}{R}\right) \quad (12)$$

The second curvature radius, along the MHP axis, is assumed to be infinite.

4.1.5. Boundary conditions

Eqs. (8)–(12) constitute a set of five coupled non-linear differential equations with five unknown variables: R, u_l, u_v, P_l and P_v. The integration begins at the cooled zone end ($x = L_\mathrm{t}$) and ends at the heated zone end ($x = 0$). At $x = L_\mathrm{t}$, the boundary conditions are as follows:

$$\begin{cases} R|_{L_\mathrm{t}} = R_\mathrm{max} \\ u_\mathrm{l}|_{L_\mathrm{t}} = u_\mathrm{v}|_{L_\mathrm{t}} = 0 \\ P_\mathrm{v}|_{L_\mathrm{t}} = P_\mathrm{sat}(T_\mathrm{v}) \\ P_\mathrm{l}|_{L_\mathrm{t}} = P_\mathrm{v}|_{L_\mathrm{t}} - \frac{\sigma}{R_\mathrm{max}} \end{cases} \quad (13)$$

where R_max is the radius of the inscribed circle in the MHP cross-section. The set of equations is solved numerically using the fourth order Runge–Kutta method. The program is stopped when $R = R_\mathrm{min}$. The position where this condition is reached corresponds to the dried length $x = L_\mathrm{d}$. In this region, the liquid does not flow anymore and the wall temperature increases rapidly.

The fluid mass is calculated in each control volume and the values are added to yield the MHP fill charge. The predicted fill charge is then compared to the experimental

one: if it is too small, a flooded length L_f is considered; if it is too large, the R_{max} curvature radius at the cooled zone end is decreased. According to the fixed fill charge and heat flux, both dry-out and flooding may occur.

4.2. Heat transfer model

The temperature profiles along the MHP are predicted by a heat transfer model [20]. The vapour temperatures are determined from the vapour pressure profile by considering a liquid–vapour equilibrium state. The wall temperatures are calculated from the thermal resistance network of the wall and the liquid film. As the dried area is large, the conductive heat transfer in the copper wall is the most important heat transfer mechanism.

5. Results

The hydrodynamic model output data are the meniscus curvature radius R, the vapour and liquid pressures, P_l and P_v, the vapour and liquid velocities, u_l and u_v. The dried length L_d is also an output data of the hydrodynamic model. The flooded length L_f is adjusted until the predicted and experimental fill charges are identical. The thermal model output data are the temperature T_{sat} and the wall temperatures. The unknown parameters, α and R_{max} are adjusted so that the predicted and experimental temperature profiles are in good accordance. The following results are given for water as working fluid, except in Section 5.2.2, in which three types of fluid are investigated.

5.1. Axial distribution of the thermo-hydraulic parameters along the MHP

In this part, the boundary conditions fixed in the model are identical to the experimental ones. The maximum meniscus curvature radius at the cooled zone end R_{max} is set to 0.75 mm (radius of the inscribed circle in the MHP), the corner angle $2\varphi_C$ is equal to 17° and the fluid fill charge is 143 mm^3. The contact angle α is varied until the experimental and predicted temperature profiles agree. A value of 64° is found, that is in good agreement with the literature data: Babin and Peterson [21] found a 55° contact angle and Nagai et al. [22] a 60° value for copper/water systems. Using these input data, the predicted dried length is of 30 mm and the flooded length of 16 mm (Fig. 4). Due to the dry-out, the whole adiabatic section acts as an evaporator, by heat conduction along the copper wall. Thus, in these operating conditions, the evaporator length is of $L_h + L_a - L_d = 15$ mm and the condenser one of $L_c - L_f = 17$ mm. The liquid cross-sectional area increases continuously from the evaporator to the condenser sections, in the same manner than the meniscus curvature radius (Fig. 5). In Fig. 6, the liquid and vapour pressure variations along the MHP are shown. The liquid pressure drops are high, especially near the evaporator end. In this region, the liquid–wall friction forces become predominant, due to the large liquid surface area in contact with the wall in comparison with the liquid cross-sectional area, which is very small. The vapour pressure drops are much smaller than the liquid ones. The vapour and liquid

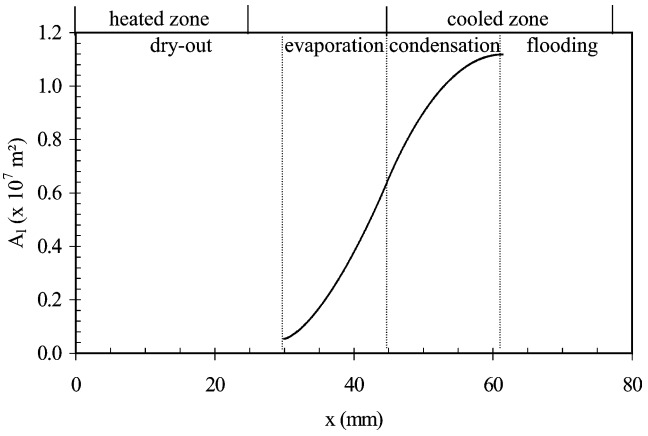

Fig. 5. Liquid cross-sectional area axial distribution ($Q = 10$ W, fill charge = 143 mm^3, $\alpha = 64°$, $R_{max} = 0.75$ mm, $2\varphi_C = 17°$).

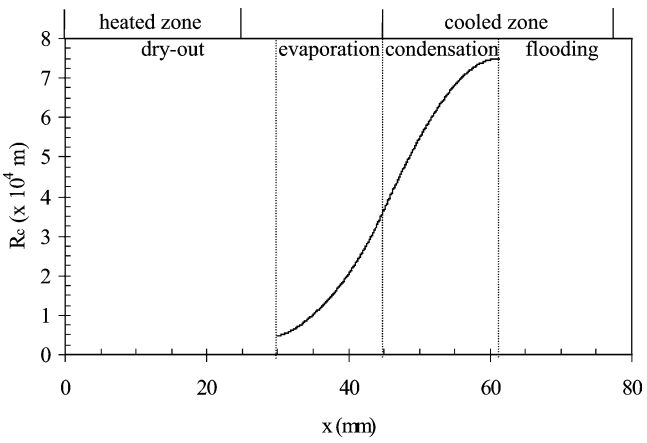

Fig. 4. Meniscus curvature radius axial distribution ($Q = 10$ W, fill charge: 143 mm^3, $\alpha = 64°$, $R_{max} = 0.75$ mm, $2\varphi_C = 17°$).

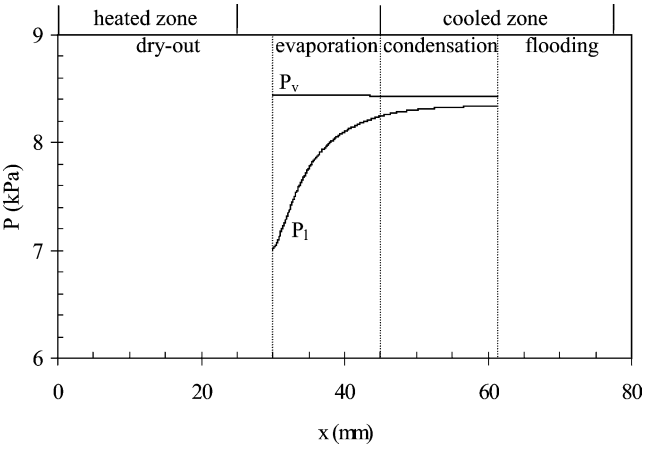

Fig. 6. Axial distribution of the liquid and vapour pressures ($Q = 10$ W, fill charge = 143 mm^3, $\alpha = 64°$, $R_{max} = 0.75$ mm, $2\varphi_C = 17°$).

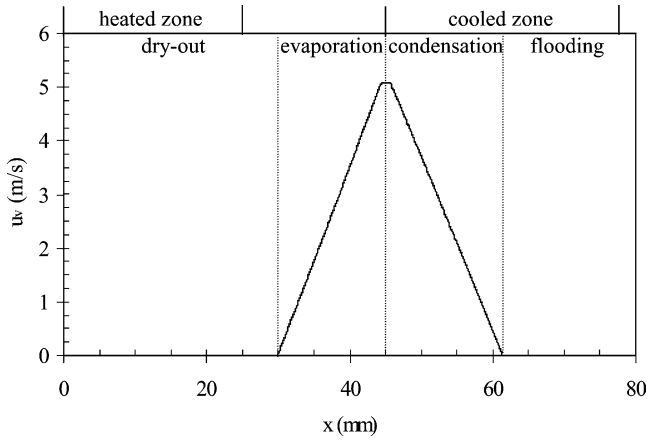

Fig. 7. Vapour velocity axial distribution ($Q = 10$ W, fill charge = 143 mm^3, $\alpha = 64°$, $R_{max} = 0.75$ mm, $2\varphi_C = 17°$).

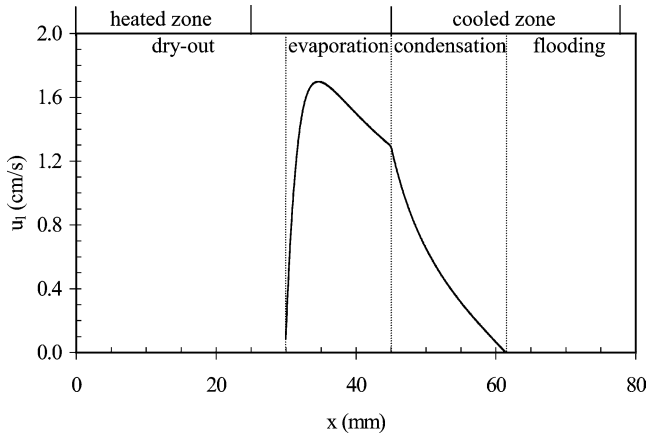

Fig. 8. Liquid velocity axial distribution ($Q = 10$ W, fill charge = 143 mm^3, $\alpha = 64°$, $R_{max} = 0.75$ mm, $2\varphi_C = 17°$).

velocities are shown in Figs. 7 and 8. The vapour velocity increases linearly in the evaporator, due to the liquid vaporisation (uniform heat flux), and decreases linearly in the condenser. The maximum vapour velocity is about 5.2 m·s^{-1}. From the condenser end, the liquid velocity increases along the condenser, due to the increasing mass flow rate. A slope discontinuity of the velocity occurs at the transition between the condenser and the evaporator. In the evaporator, the mass flow rate and the liquid cross-sectional area decrease simultaneously. Thus, the variation of the liquid velocity will depend on the relative variations of these parameters. Near the evaporator end, as A_l decreases more rapidly than the mass flow rate, u_l decreases too. The liquid velocity reaches a maximum value of about 1.6 cm·s^{-1} in the evaporator.

A comparison between the experimental data and the theoretical results for the temperature distribution along the MHP is shown in Fig. 9. In this figure, the experimental data agree very well with the model for the charged MHP. This agreement is not so good for the adiabatic zone of the empty MHP. The maximum wall temperatures for the filled and empty MHPs are about of 110 °C and 131 °C, respectively.

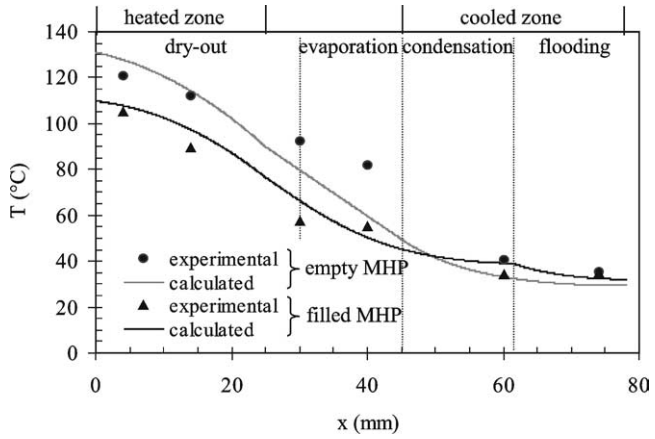

Fig. 9. Comparison of the experimental and calculated temperatures for the charged and empty MHPs ($Q = 10$ W).

In the previous investigations, it was assumed that the MHP array was perfectly thermally insulated. Thus, the whole heat input (10 W) is transferred through the MHP. In the experimental conditions, there might be some heat losses to the environment. The calculated heat losses are about 5% of the heat input. With these heat losses and for $2\varphi_C = 17°$ and $R_{max} = 0.75$ mm, the contact angle is varied until experimental and predicted temperatures agree. The predicted contact angle is of 66° instead of 64° for a 10 W heat input. Therefore, the effect of heat losses on the results presented here is negligible.

5.2. Prediction of the MHP capillary limit

The maximum heat flux Q_{max} corresponding to the capillary limit is reached when the liquid distribution in the MHP is such that the meniscus curvature radius is minimum at the heated zone beginning ($x = 0$) and maximum at the cooled zone end ($x = L_t$). In this configuration, where no dry-out and no flooding occur inside the MHP, the fluid fill charge is optimal. In the model, the maximum curvature radius at the cooled zone end is fixed to 0.75 mm and Q is varied until reaching the minimum curvature radius at the heated zone end. The corner angle is set to 17° and the contact angle to 64°. The predicted maximum heat transfer rate is 1.5 W (0.61 W·cm^{-2}) and the optimum fill charge is of 25 mm^3.

The corresponding temperature profile of the charged MHP, which is deduced from the calculated vapour pressure, is very flat (Fig. 10). This temperature profile is compared to the temperature profile of an empty copper MHP and of a pure copper bar with identical external dimensions. The maximum temperature differences along the empty heat pipe and the bar are 14 K and 9 K, respectively (Fig. 10). It is clearly shown that, under these operating conditions, the thermal performances of the charged heat pipe are better and allow to transfer heat fluxes with low temperature differences.

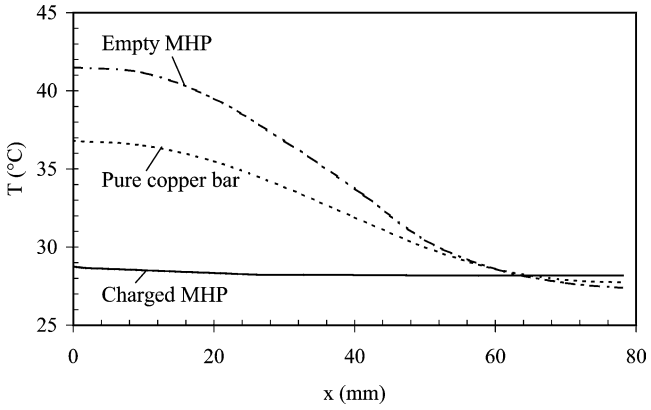

Fig. 10. Comparison of the calculated temperatures for the charged MHP, the empty MHP and a pure copper bar ($Q = 1.5$ W).

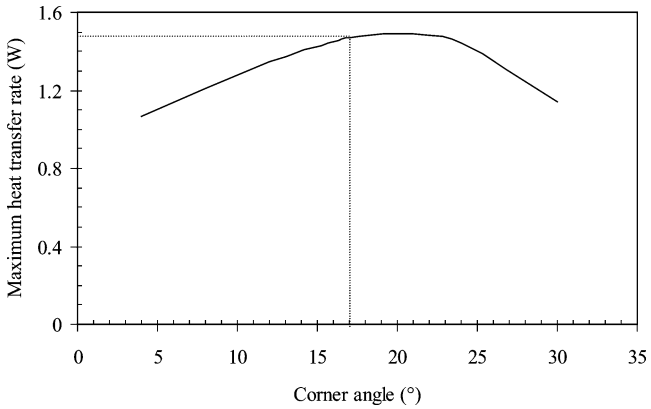

Fig. 11. Effect of the corner angle on the MHP capillary limit.

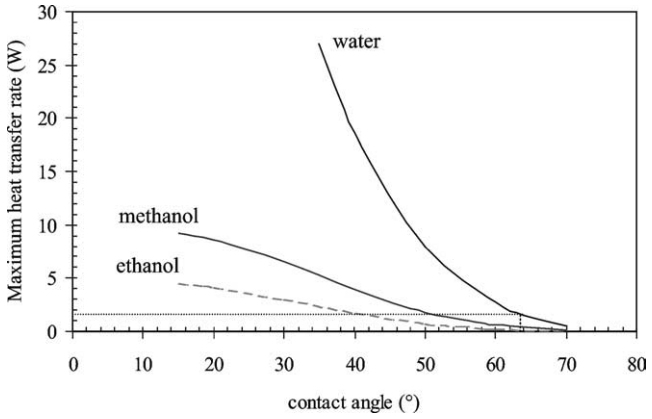

Fig. 12. Effect of the contact angle on the MHP capillary limit, charged with water, methanol or ethanol.

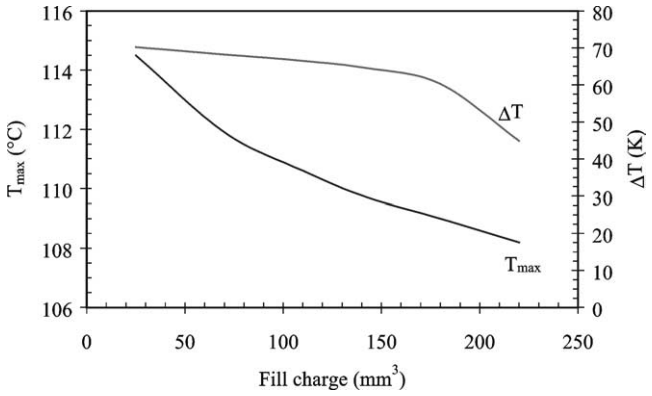

Fig. 13. Effect of the fluid fill charge on the maximum wall temperature and on the maximum wall temperature difference ($Q = 10$ W).

5.2.1. Effect of the corner angle on the capillary limit

The effect of the corner angle on the MHP capillary limit is shown in Fig. 11. The $Q_{\max}$ value of 1.5 W is reached for corner angles ranging between 17 and 24°. For decreasing corner angle ($2\varphi_C < 17°$), $Q_{\max}$ decreases due to increasing liquid–wall friction forces in the region located near the corner apex. For increasing corner angle ($2\varphi_C > 24°$), $Q_{\max}$ decreases due to the decreasing cross-sectional area available for the liquid, inducing a decreasing liquid mass flow rate in the corner region.

5.2.2. Effect of the contact angle on the capillary limit

This investigation aims to study the contact angle effect on the MHP performance. The maximum heat transfer rate corresponding to the capillary limit is calculated as a function of the contact angle, for water, methanol or ethanol as working fluids (Fig. 12). For the three fluids, the maximum heat transfer rate increases as the contact angle decreases but in the case of methanol and ethanol, the curves level off at low contact angles. For a given contact angle, the MHP capillary limit is higher using water than the alcohols, due to their thermophysical properties. Especially, the latent heat of vaporisation of water is greater than the methanol one, that is itself greater than the ethanol one. For a same fluid flow rate, the heat transfer rate decreases with h_{lv}. In addition, for ethanol, the liquid dynamic viscosity and consequently, the liquid pressure drops, are greater than for methanol. These curves also show that the selection of a fluid depends on its contact angle. If the copper/water contact angle is equal to 64° , the methanol and ethanol MHPs would have better performances than water if their contact angles are lower than 52° and 42°, respectively.

5.3. Effect of the fill charge on the temperature profile

The effect of the fill charge on the MHP maximum wall temperature is shown in Fig. 13, for $Q = 10$ W. This heat transfer rate is above the capillary limit that has been previously calculated, $Q_{\max} = 1.5$ W. As a result, whatever the fluid fill charge, a more or less large part of the evaporator section is dried out. When the fill charge increases, the dried surface area decreases and the evaporator thermal resistance too. But, simultaneously, the liquid in excess is blocked at the condenser end, leading to an increase of the flooded region, which does not participate in heat transfer. Thus, the condenser thermal resistance increases. In the studied fill charge range, the maximum wall temperature difference ΔT decreases with an increasing fluid fill charge, pointing out a decrease of the MHP total thermal resistance

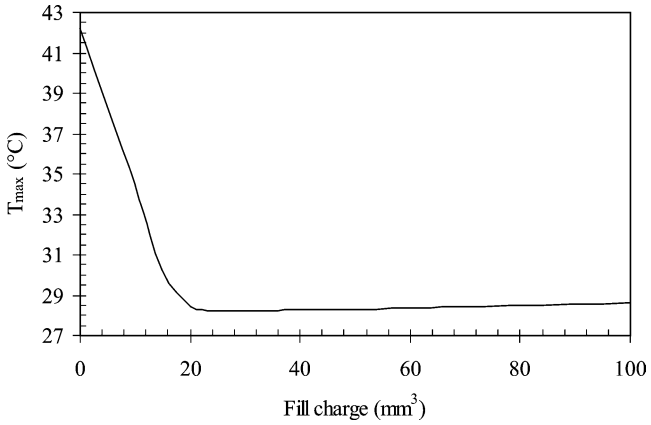

Fig. 14. Effect of the fluid fill charge on the maximum wall temperature ($Q = Q_{max}$).

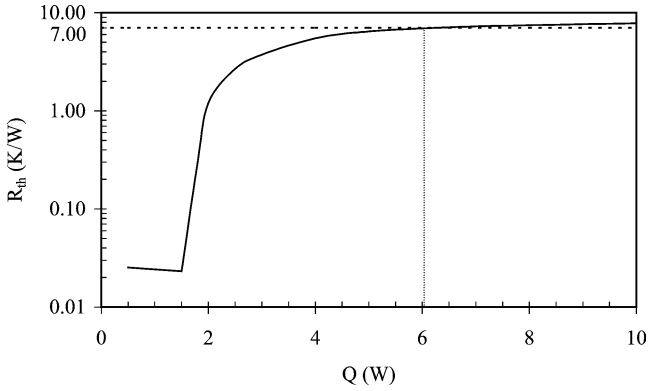

Fig. 15. Effect of the heat input on the MHP thermal resistance.

(Fig. 13). As the condenser wall temperature does not vary with the fill charge, the maximum wall temperature of the evaporator decreases too. For higher charges, as the condensing surface area becomes smaller and smaller, the condenser thermal resistance increase will be greater to the decrease of the evaporator one, leading to a MHP thermal resistance increase. The condenser is totally flooded for fill charges greater than 273 mm^3.

For $Q = Q_{max}$, the effect of the fill charge on the MHP maximum wall temperature is shown in Fig. 14. T_{max} has a minimum value for the optimum fill charge, i.e., 25 mm^3. For larger fill charges, T_{max} slightly increases because the condenser flooding leads to an increase of the MHP thermal resistance. For low fill charges, T_{max} increases steeply, due to the evaporator dry-out.

5.4. Effect of the heat input on the MHP performance

The effect of the heat input on the MHP array performance is shown in Fig. 15. The minimum value of the thermal resistance of the MHP (0.02 K·W^{-1}), which corresponds to the maximum thermal performance of the MHP array, is reached for the MHP capillary limit (1.5 W). Above the capillary limit, dry-out occurs. Thus, the temperature difference along the MHP increases more than the heat input increase, leading to a MHP thermal resistance increase for high heat fluxes. The thermal resistance of the empty MHP and the copper bar are equal to 10 K·W^{-1} and 7 K·W^{-1}, respectively. Consequently, for heat fluxes greater than 6 W, a MHP presents no interest compared to a copper bar.

6. Conclusion

In this work, a copper/water wire plate MHP array, of external dimensions 78 × 10 × 2 mm^3, which has been fabricated with a diffusion welding process, has been investigated. This new technology is promising, due to the quality of the corners obtained. Experimental and numerical investigations were carried out to study the thermal performance of this device. The results have shown that its effective thermal conductivity is improved by a factor 1.3 as compared to the empty MHP array. A numerical model has been developed to predict the capillary limit and the temperature profile of the MHP array for fixed boundary conditions, at a fixed fill charge or at the optimum fill charge. A good agreement between the theoretical and experimental data has been obtained.

This MHP geometry is interesting, since it is able to operate with low wetting fluids (contact angle 60–70°). However, the maximum heat flux corresponding to the capillary limit is low in this case, 0.61 W·cm^{-2}. Thus, further developments are necessary to improve the MHP performance, by optimising its geometry or using other fluids.

References

[1] M. Lallemand, V. Sartre, A review of the recent research and development on micro heat pipes, in: Compact Heat Exchanger Symposium, Grenoble, France, August 24 2002.
[2] D. Plesch, W. Bier, D. Seidel, K. Schubert, Miniature heat pipes for heat removal from microelectronic circuits, in: Micromech. Sensors, Actuators and Systems ASME-DSC, vol. 32, 1991, pp. 303–314.
[3] L.H. Chien, M.H. Kuo, Experiments and prediction of capillary limits for integrated plat heat pipes, in: 35th AIAA Thermophysics Conference, Anaheim, California, 2001.
[4] Y.X. Wang, G.P. Peterson, Analysis of wire-bonded micro heat pipe arrays, J. Thermophysics and Heat Transfer 16 (3) (2002) 346–355.
[5] M.B.H. Mantelli, A.J.A. Buschinelli, R.M. Nascimento, K.V. Paiva, Diffusion welding of wire micro heat pipe arrays, in: 12th IHPC, Mocow–Kostroma–Moscow, Russia, May 19–24, 2002, 6 p.
[6] G.P. Peterson, A.B. Duncan, M.H. Weichhold, Experimental investigation of micro heat pipes fabricated in silicon wafers, J. Heat Transfer 115 (1993) 751–756.
[7] S. Launay, V. Sartre, M. Lallemand, Banc d'essais de microcaloducs en technologie silicium, in: 5ème Colloque Franco-Québécois, Lyon, 28–30 mai, 2002, pp. 223–229.
[8] B. Badran, F.M. Gerner, P. Ramadas, T. Henderson, K.W. Baker, Experimental results for low-temperature silicon micromachined micro heat pipe arrays using water and methanol as working fluids, Exp. Heat Transfer 10 (1997) 253–272.
[9] S.W. Kang, S.H. Tsai, H.C. Chen, Fabrication of micro radial grooved heat pipes, in: 12th IHPC, Mocow–Kostroma–Moscow, Russia, 19–24 May, 2002, 6 p.

[10] American Welding Society, Welding Handbook, vol. 2, seventh ed., 1978.
[11] A.E. Martinelli, Diffusion Bonding of Silicon Carbide and Silicon Nitride to Molybdenum, McGill University, 1996.
[12] R. Lison, Diffusionschweissen une seine Andendung Beispiele aus der Kerntechnik, Schweisse und Schneiden 18 (8) (1971) 304–308.
[13] T.P. Cotter, Principles and prospects for micro heat pipes, in: 5th IHPC, vol. 4, Tsukuba, Japan, 1984, May 14–18, pp. 328–334.
[14] M.C. Zaghdoudi, V. Sartre, M. Lallemand, Theoretical investigation of micro heat pipes performance, in: 10th IHPC, Stuttgart, Germany, 21–25 September 1997, 6 p.
[15] S. Launay, Performances thermiques de microcaloducs usinés dans du silicium. Modélisation et étude expérimentale, Ph.D. Thesis, INSA, Lyon, France, 2002.
[16] J.P. Longtin, B. Badran, F.M. Gerner, A one-dimensional model of a micro heat pipe during steady-state operation, J. Heat Transfer 116 (1994) 709–715.
[17] G.P. Peterson, H.B. Ma, Theoretical analysis of the maximum heat transport in triangular grooves: a study of idealized micro heat pipes, J. Heat Transfer 118 (1996) 731–739.
[18] B.R. Babin, G.P. Peterson, D. Wu, Steady-state modeling and testing of a micro heat pipe, J. Heat Transfer 112 (1990) 595–601.
[19] D. Wu, G.P. Peterson, W.S. Chang, Transient experimental investigation of micro heat pipes, J. Thermophys. 5 (1991) 529–544.
[20] S. Launay, V. Sartre, M. Lallemand, Thermal study of a water-filled micro heat pipe including heat transfer in evaporating and condensing microfilms, in: 12th International Heat Transfer Conference, Grenoble, France, August 18–23 2002, 6 p.
[21] G.P. Peterson, B.R. Babin, Analytical and experimental investigation of miniature heat pipes—Phase II, Final Report WRDC-TR-89-2067, 24 June 1989, 64 p.
[22] N. Nagai, M. Takeuchi, T. Kimura, T. Kanashima, Attempts for measuring contact angles on superheated walls, in: 11th IHTC, vol. 4, Kyongyu, Korea, August 23–28 1998, pp. 137–141.